DSN–MVM'73 S/X Dual-Frequency Doppler Demonstration During Superior Conjunction

K. W. Yip, F. B. Winn, and S. J. Reinbold
Tracking and Orbit Determination Section

During the Mariner Venus/Mercury 1973 (MVM'73) mission, the S/X dual-frequency doppler calibrations (for plasma and ionospheric charged-particle dynamics) have been demonstrated to improve post-flight radio metric doppler reductions: the error of one Mercury I encounter position estimate was reduced by 500 km (~ 80%). This demonstration used tracking data acquired from March 16–29, 1974. The Sun–Earth–probe angle (SEP) was greater than 30 deg during this time.

As the SEP decreases, S/X calibrations indicate dramatic increases in plasma dynamics. Simultaneously, the noises of the S and X dopplers and the S/X calibrations increase by 2 orders of magnitude as the SEP decreases from 30 to 3 deg. When these calibrations are used to support Mariner 10 navigation, unreasonable results are obtained. The calibrations, their noise characteristics, and their impact on Mariner 10 navigation are herein outlined.

One possible cause for this behavior is that multi-pathing of radio signals to Mariner 10 produces phase scintillations of the S-band uplink transmission in excess of $\pi/2$ rad/s (3.5 cm of integrated phase change per second). This probably exceeds the linear performance region of the second-order phase-locked loops.

I. Introduction

The successful demonstration of the S/X dual doppler experiment for the pre-Mercury I phase of MVM'73 has been reported in Ref. 1. This article reports on the status of the demonstration around the superior conjunction period from May 27 through June 9, 1974.

A study of the superior conjunction S/X dispersive doppler reveals that those data are excessively noisy

(approximately 0.5 Hz). Moreover, when the derived charged-particle information was applied in the orbit determination (OD) process, the resultant statistics were seriously degraded and the second Mercury B plane solution was moved by an unreasonably large amount from the uncalibrated solution, which was in fair agreement with the best pre-trajectory correction maneuver 5 (TCM5-July 2) estimates.

In the following paragraphs, the characteristics of the S/X calibrations will be investigated and the data noise will be discussed. The orbit determination results for this data arc will be briefly presented, and, finally, a report will be made on the status of the investigation into the origin of the noise.

II. Noise Characteristics of the S/X Dispersive Doppler Calibrations

To put the entire S/X dual doppler demonstration (up through June 9) in perspective, let us begin with a study of the noise characteristics of the pre-Mercury I S/X charged-particle calibrations. Figure 1 shows the noise characteristics for the March 24, 1974 pass. This is one of the passes from the successful pre-Mercury I charged-particle demonstration. Application of S/X calibrations to this 9-day arc improved the quality of the doppler fit by reducing the sum of the squares of the doppler residuals by over 70%. Also, errors were diminished by 80% for one Mercury I encounter plane position estimate, based on a data set for which calibrations exist.

Figure 1 displays the S/X dispersive doppler calibrations (*) and the mean and one-sigma values as obtained from a 20-point running average through the calibrations. Note that the vertical scale is in millihertz, and, as indicated, the noise of the S/X calibration is about 2 mHz on this day. This is typical of the noise characteristics for the pre-Mercury I S/X dual-frequency doppler.

Figure 2a shows the noise characteristics for a typical day in the superior conjunction phase of the MVM'73 mission. Note, however, that the vertical scale is in hertz and the noise characteristics for this day are, therefore, at least two orders of magnitude larger than those on the pre-Mercury I days. It is also evident that the amplitude of the S/X doppler noise is not stationary. Figure 2b shows the March 24 pass plotted on the one-hertz scale.

Figure 3 displays the noise characteristics of the S/X dispersive doppler charged-particle calibrations for a few days between March 24 and June 7, 1974. Note that the scatter increases as the SEP angle decreases (Fig. 4).

III. Demonstration That the Superior Conjunction S/X Doppler Calibration Is No Reflection on Charged Particles

Figures 5, 6, and 7 display the unedited S- and X-band doppler residuals after the removal of the effects of the spacecraft trajectory and Earth's troposphere. Figure 8 shows the ratio of the noise of the X-band to that of the S-band residuals. Again these ratios have been obtained by 20-point running averages. For significant fractions of these passes, these ratios of the rms noises are larger than four. This is an important observation. The S/X experiment, as configured for Mariner 10, has only an S-band uplink capability. The X-band downlink retransmitted by the spacecraft is obtained by multiplying the S-band uplink by 880/221 (approximately a factor of 4). The charged-particle effect on the X-band is approximately 1/16 that of the S-band. Consequently, even if there is no charged-particle effect on the S-band downlink signal, the ratios as computed should be *at most four.* In other words, considering only plasma-induced noise, the relative rms noise of the X- and S-band dopplers transmitted from the spacecraft is 4 to 1, and, if the downlink S-band doppler is further scintillated by plasma dynamics, the ratio decreases. Thus, it is obvious that the high frequency variations of the dopplers are not due to charged-particle content fluctuations.

The following analysis again confirms that the "charged-particle" calibrations derived from the superior conjunction S/X dispersive doppler data do not accurately reflect the line-of-sight charged-particle dynamics. Figures 9, 10, and 11 show the S-band tracking doppler residuals before and after the application of the calibrations. The S-band residuals are of the order of 100 mHz, except for the June 7 pass when they are as large as 200 mHz. However, without exception, they become significantly larger after calibrations. This demonstrates that the S/X calibrations of the superior conjunction phase quality cannot remove the charged-particle effect. In fact, noise has been added to the doppler residuals—a noise which is not stationary.

IV. Orbit Determination Results

Since the calibrations derived from the S/X dispersive doppler data do not accurately reflect the line-of-sight charged-particle effects, when they are applied to the orbit determination process, unreasonable results are obtained. Figure 12 shows the OD results for the "state only" solution with and without calibrations. Whereas the uncalibrated B-plane solution is fairly close to the pre-TCM5 current best estimate ($\mathbf{B}\cdot\mathbf{R} \cong 24{,}000$ km, $\mathbf{B}\cdot\mathbf{T} \cong -24{,}050$ km), the calibrated estimate is displaced from the

B·R values by approximately 10,000 km. The sum of squares of the after-the-fit doppler residuals is increased by almost a factor of 20 when calibrations are applied. As illustrated in Figs. 9, 10, and 11, the calibrations have degraded the S-band residuals by imparting to them the large noise signatures that are in the S/X dispersive doppler data.

V. Status on the Investigation of Possible Noise Origins

The rms noise of S-band doppler increases dramatically as the SEP angle of the probe decreases (Fig. 13) below 10 deg. Similar behavior was observed in the Mariner 10 (Fig. 13), Mariner 9 (Fig. 13), Mariners 6 and 7 (Ref. 2), and in the Pioneer 10 and 11 (Fig. 13) S-band doppler data.

D. O. Muhleman (Ref. 3) computed the rms phase jitter of S-band frequency transmissions from plasma amplitude scintillation observations and scintillation theory. The curve containing the shaded area (Fig. 13) is the theoretical rms noise as a function of SEP angle computed by Muhleman.

The S-band doppler rms observed is 5- to 6-fold greater than the rms predicted if the SEP angle region of ±3 deg is excluded from consideration. It is an order of magnitude greater than that predicted in the ±3-deg zone.

One possible explanation for this is suggested from the knowledge that spacecraft radio tracking systems employ "second-order phase-locked loops" (Ref. 4). Such loops require less than $\pi/2$-rad phase jitter in the pass bands (Ref. 3) if they are to remain in "uninterrupted" phase lock. That is, the signal received by such a system must have coherence for time scales on the order of a second. $\pi/2$ rad of phase shift at S-band frequencies amounts to approximately 3.5 cm. A change in the total electron content along the ray path of 5×10^{15} electrons/m^2 is required. Variations of electron content far larger than these have been observed (Ref. 5). It is reasonable to assume that electron content dynamics larger than 5×10^{15} electrons/m^2/s were encountered by the Mariner 10 radio metric doppler. When such dynamics are encountered by a radio signal at S-band frequencies, the domain of linear performance of the radio tracking system may be exceeded. Note further that the doppler noise shown in Fig. 13 is roughly consistent with the 3.5-cm short-term instability.

The X-band transmission leaving the spacecraft is obtained by multiplying the spacecraft-received S-band by 880/221. Since this is an exact process, this X-band transmission has approximately 4 times the phase jitter of the S-band transmission. If the spacecraft-tracked S-band doppler contains cycle slips, then the spacecraft-transmitted X-band doppler may exceed the linear performance domain of ground receivers.

How a "linear receiving system" responds to such S- or X-band signals with such spectral characteristics may be shown:

(1) Theoretically by studying the "mathematical model of second-order loops" and how they respond to real and simulated data of the type encountered during the Mariner 10 superior conjunction.

(2) Empirically by passing wide-band doppler through the DSS 14 Block 4 receiver.

VI. Conclusion

Our experience with the S/X dual-frequency doppler demonstration for the pre-Mercury I phase was very promising. For the superior conjunction period of the mission, during which the charged-particle activities are very high, the X-band downlink only configuration is incapable of providing meaningful charged-particle calibrations.

References

1. Winn, F. B., Yip, K. W., and Reinbold, S. J., "DSN-MVM'73 S/X Dual-Frequency Doppler Demonstration," in *The Deep Space Network Progress Report 42-22*, pp. 28–50, Jet Propulsion Laboratory, Pasadena, Calif., Aug. 15, 1974.

2. Esposito, P. B., *Helios-Investigation of the Solar Corona and Relativistic Time Delays During Superior Conjunction*, TM 391-478, Aug. 22, 1973 (JPL internal document).

3. *Proceedings of the Conference on Experimental Tests of Gravitation Theories*, California Institute of Technology, Pasadena, Calif., Nov. 1970.

4. *Telecommunication System Design Techniques Handbook*, Technical Memorandum 33-571, Jet Propulsion Laboratory, Pasadena, Calif., July 15, 1972.

5. Brandt, J. C., *Introduction to the Solar Wind*, pp. 133–134, W. H. Freeman and Co., 1970.

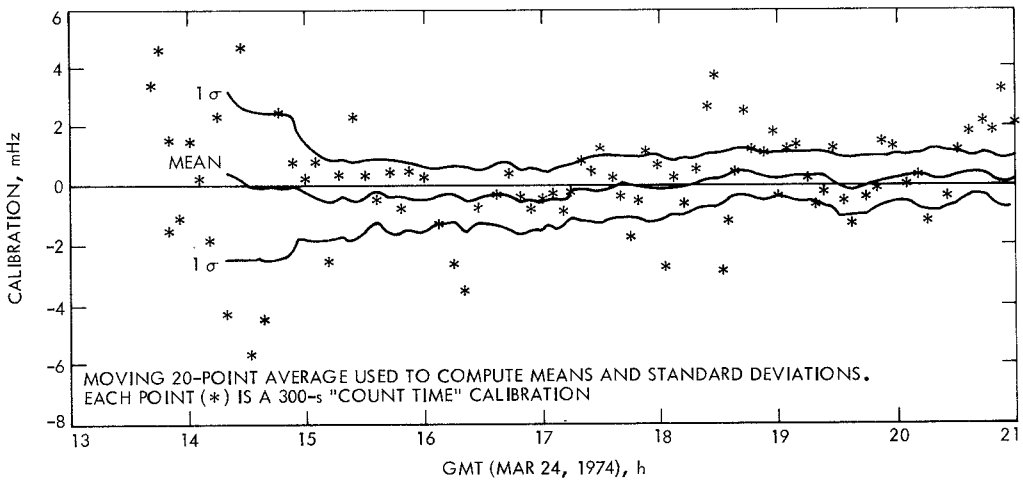

Fig. 1. Typical S/X dual doppler, charged-particle calibrations, and associated noise characteristics for the pre-Mercury I phase

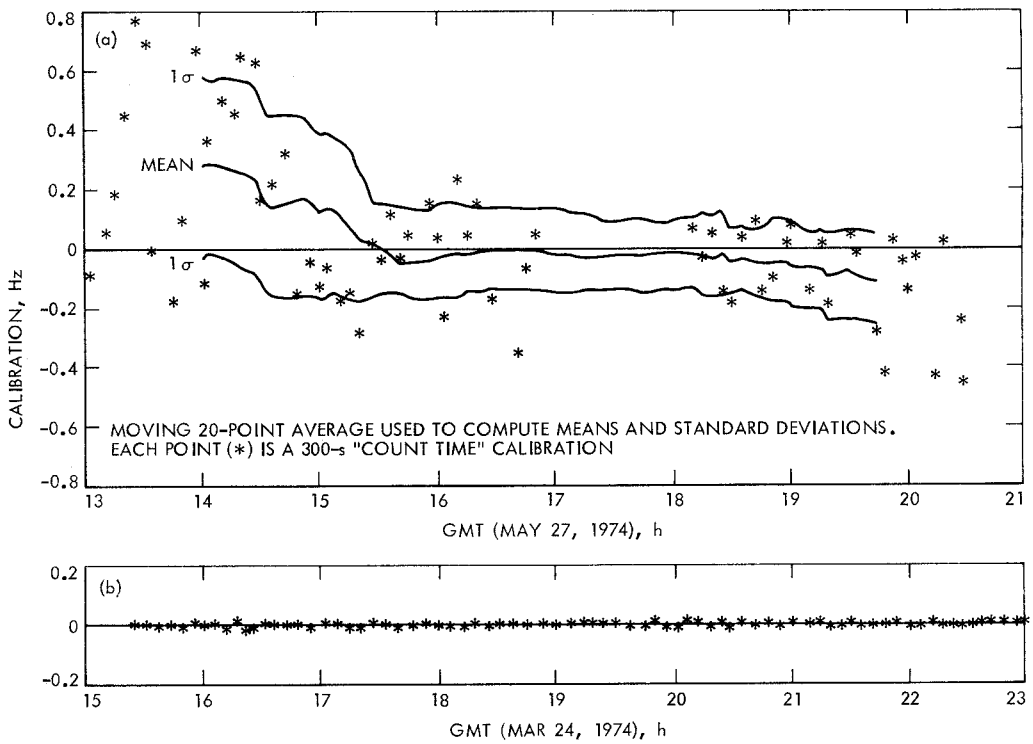

Fig. 2. Comparison of S/X dual doppler, charged-particle calibrations, and associated noise characteristics for the pre-Mercury I phase and superior conjunction phase

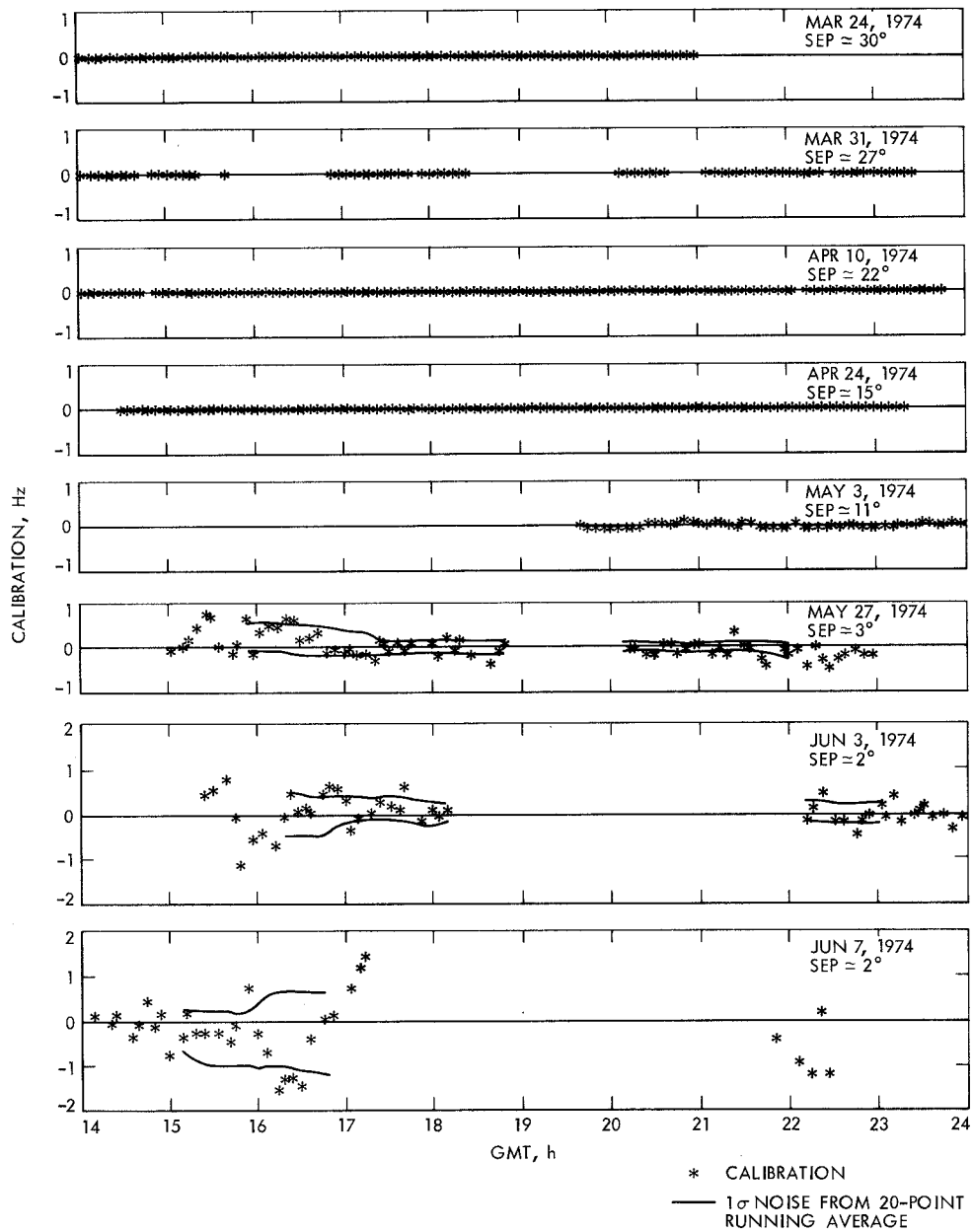

Fig. 3. Noise characteristics of S/X dual doppler charged-particle calibrations

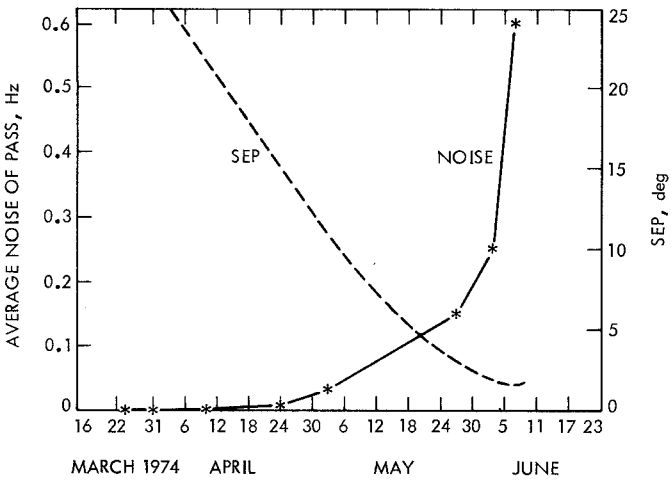

Fig. 4. Noise in S/X doppler calibrations vs SEP angle

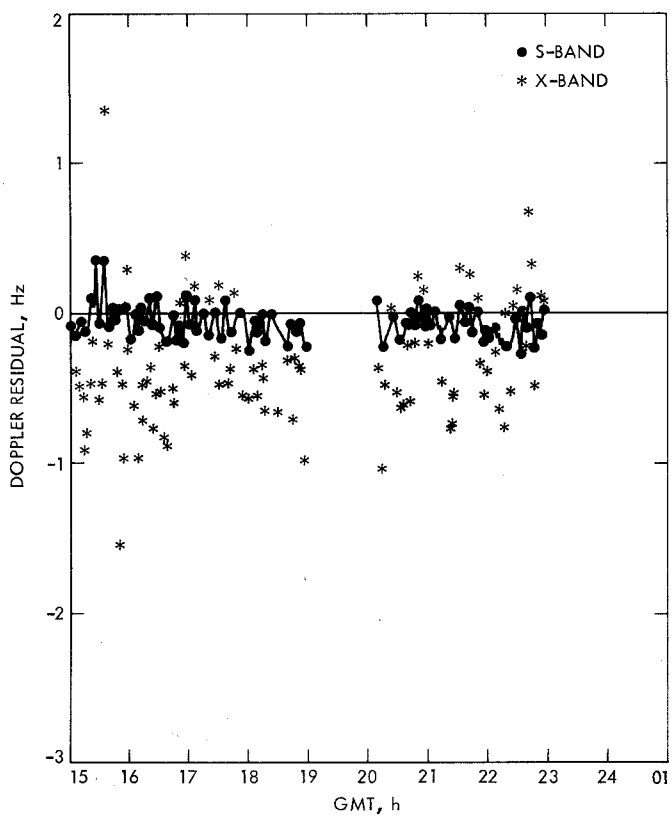

Fig. 5. S- and X-band doppler residuals for May 27, 1974

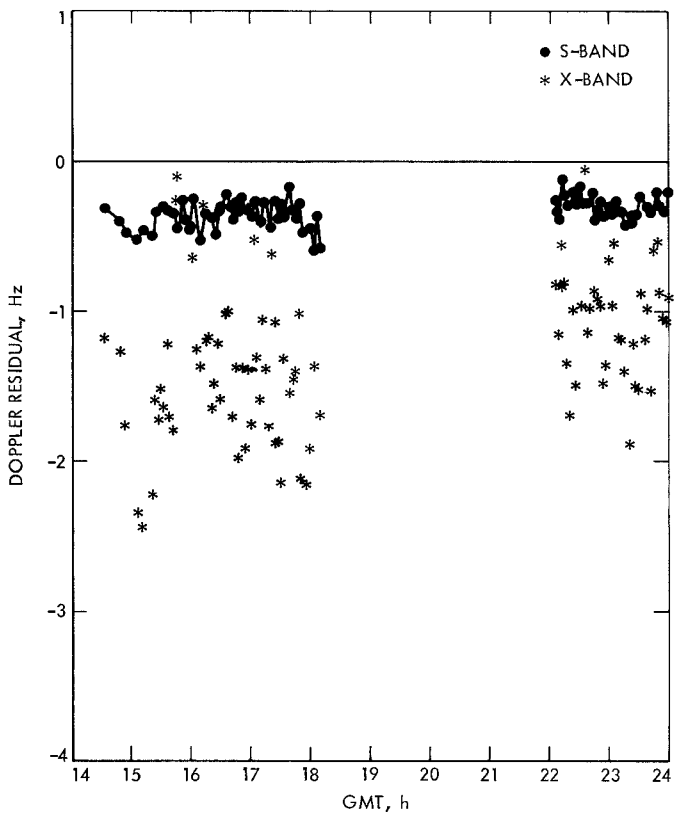

Fig. 6. S- and X-band doppler residuals for June 3, 1974

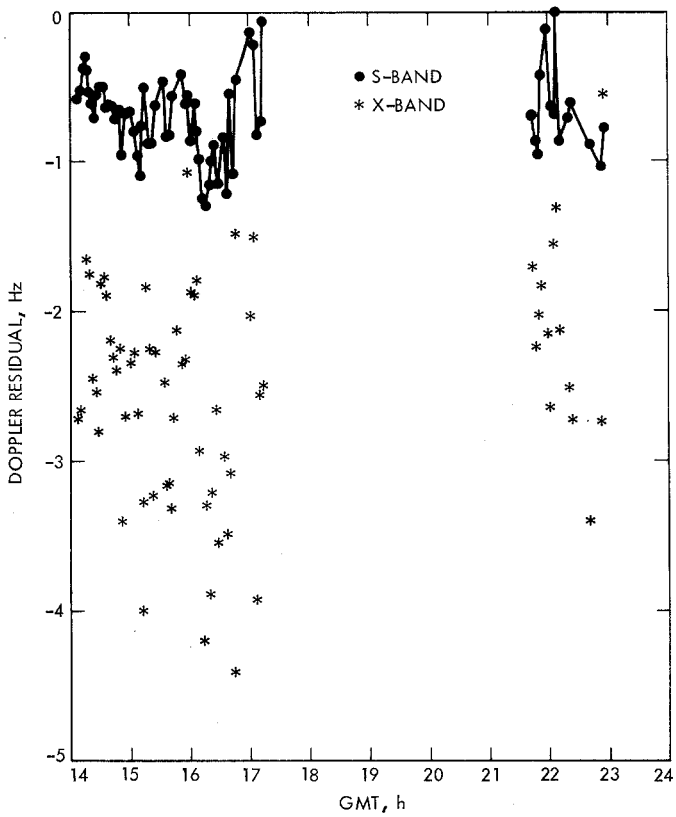

Fig. 7. S- and X-band doppler residuals for June 7, 1974

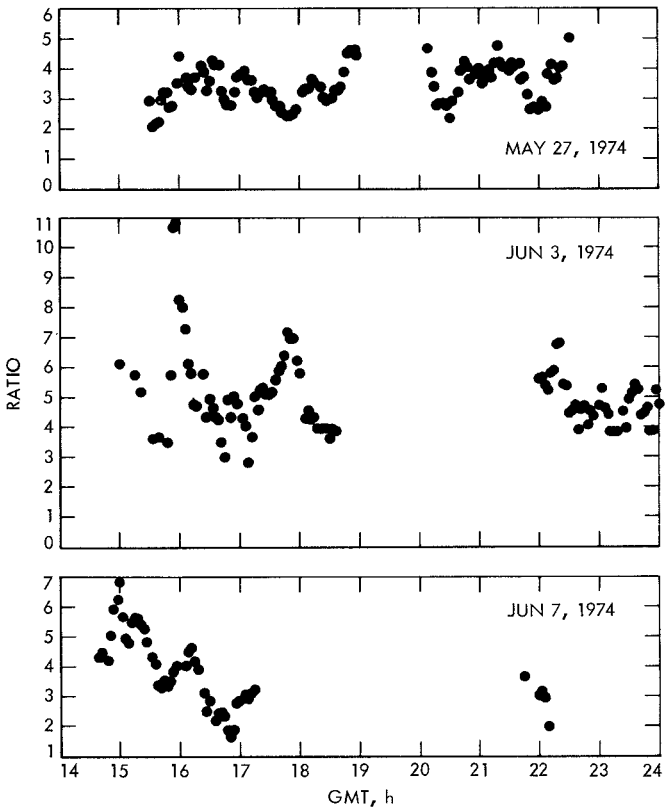

Fig. 8. Ratio of X-band to S-band doppler residual noise

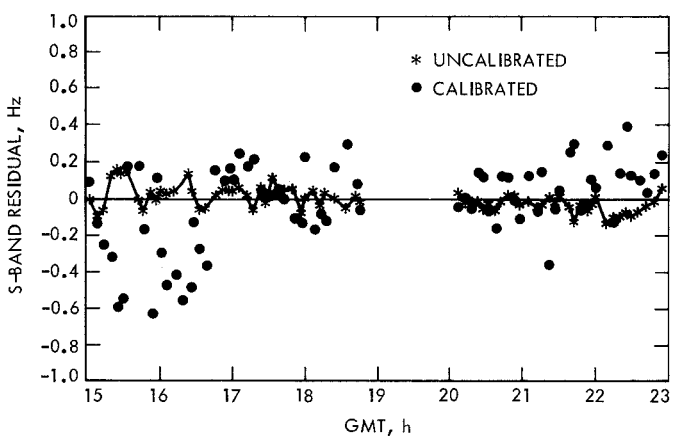

Fig. 9. Calibrated and uncalibrated S-band tracking doppler residuals (after the fit) for May 27,1974

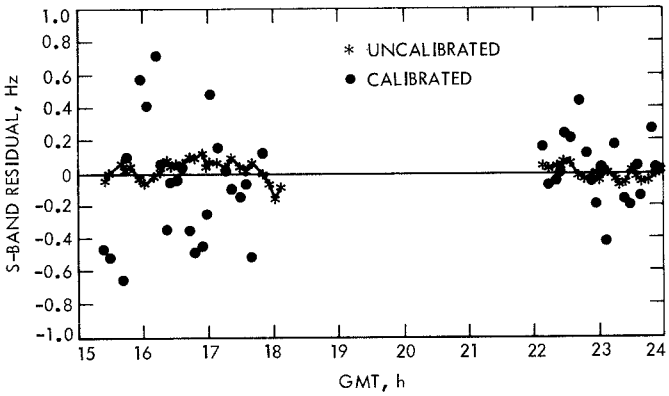

Fig. 10. Calibrated and uncalibrated S-band tracking doppler residuals (after the fit) for June 3, 1974

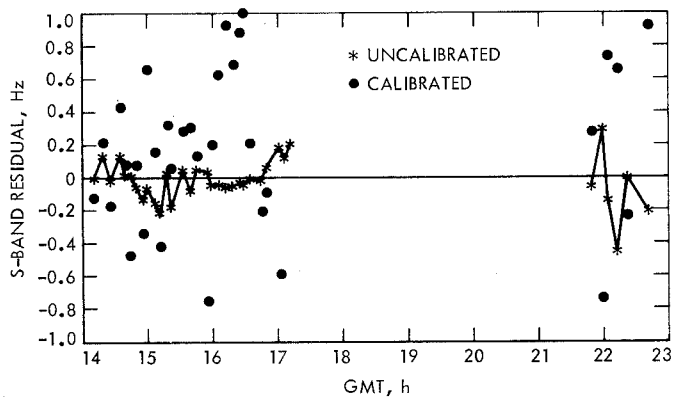

Fig. 11. Calibrated and uncalibrated S-band tracking doppler residuals (after the fit) for June 7, 1974

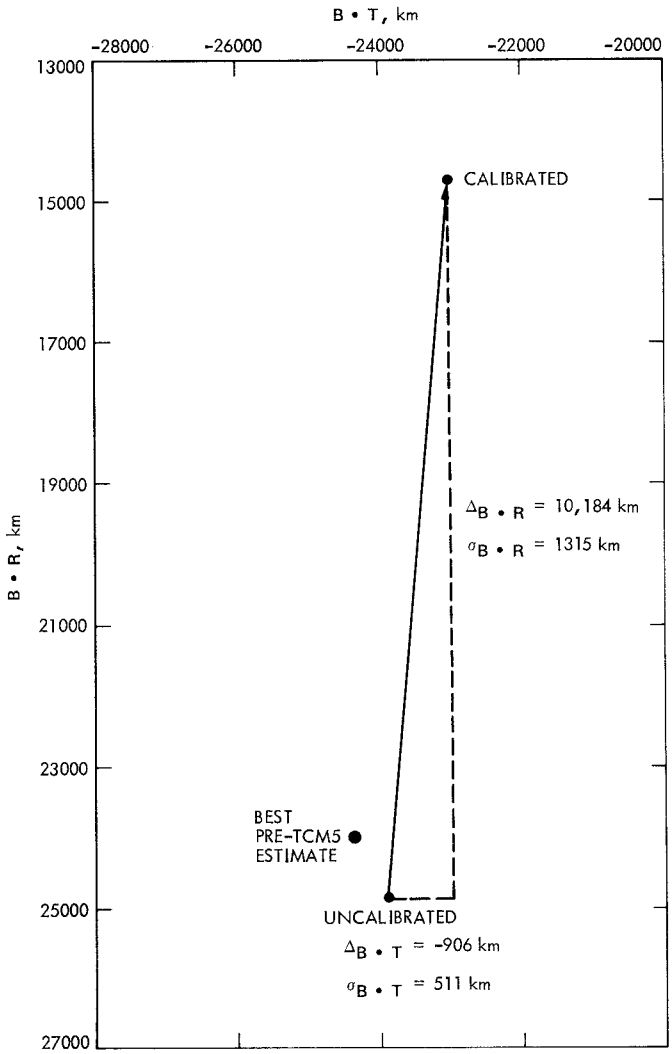

Fig. 12. Pre-TCM5 MVM'73 Mercury II encounter plane coordinate estimates: impact of superior conjunction S/X calibrations

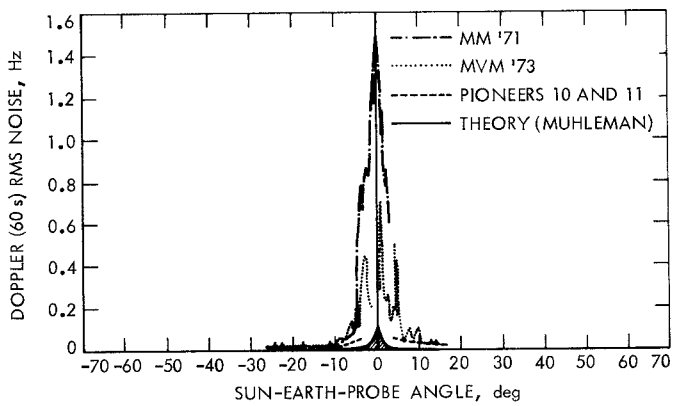

Fig. 13. Rms noise of S-band doppler vs SEP angle